



Trans. Nonferrous Met. Soc. China 35(2025) 3443-3454

Transactions of Nonferrous Metals Society of China

www.tnmsc.cn



MIL-100(Fe) decorated TiO₂ for robust hydrogen storage in magnesium hydride

Ren ZHOU¹, Li WANG¹, Tao ZHONG¹, Shuai LI¹, Dong-qiang GAO¹, Fu-ying WU², Liu-ting ZHANG¹

- 1. School of Energy and Power, Jiangsu University of Science and Technology, Zhenjiang 212003, China;
- 2. Instrumental Analysis Center, Jiangsu University of Science and Technology, Zhenjiang 212003, China

Received 27 January 2024; accepted 21 October 2024

Abstract: To modify the stable thermodynamics and poor kinetics of magnesium hydride (MgH₂) for solid-state hydrogen storage, MIL-100(Fe) was in situ fabricated on the surfaces of TiO₂ nano-sheets (NS) by a self-assembly method, and the prepared TiO₂ NS@MIL-100(Fe) presents an excellent catalytic effect on MgH₂. The MgH₂+ 7wt.%TiO₂ NS@MIL-100(Fe) composite can release hydrogen at 200 °C, achieving a decrease of 150 °C compared to pure MgH₂. Besides, the activation energy of dehydrogenation is decreased to 70.62 kJ/mol and 4 wt.% H₂ can be desorbed within 20 min at a low temperature of 235 °C. Under conditions of 100 °C and 3 MPa, MgH₂+7wt.%TiO₂ NS@MIL-100(Fe) absorbs 5 wt.% of H₂ in 10 min. Surprisingly, 6.62 wt.% reversible capacity is maintained after 50 cycles. The modification mechanism is confirmed that the presence of oxygen vacancies and the synergistic effect of multivalent titanium in TiO₂ NS@MIL-100(Fe) greatly enhance the kinetic and thermodynamic properties of MgH₂. **Key words:** hydrogen storage; magnesium hydride; oxygen vacancies; multivalent titanium; catalytic mechanism

1 Introduction

As the global energy crisis and environmental problems intensify, energy has become an important factor limiting the development of countries around the world [1-3]. With its high calorific value, cleanliness, and wide range of sources, hydrogen energy is considered as an ideal energy to replace fossil fuels [4-6]. However, hydrogen storage, which serves as a bridge between hydrogen production and applications, greatly hinders the large-scale application of hydrogen energy [7,8]. Among many hydrogen storage materials, MgH₂ has attracted a lot of attention from researchers due to its excellent volumetric density (110.0 kg/m³) and gravimetric hydrogen density (7.6 wt.%) [9–11]. However, strong metal - hydrogen bonds and kinetic barriers restricted its further development

and practical applications. To solve this challenge, researchers have taken a variety of approaches, and the common types include nanosizing [12,13], alloying [14–16], and catalyzing [17–19].

TiO₂ with its tunable Ti valence state and crystalline surface, is an excellent catalyst for raising the hydrogen storage capacity of MgH₂ [20–22]. CROSTON et al [23] found that the hydrogen desorption temperature of TiO₂ doped MgH₂ (257 °C) was lowered by 100 °C. Although the dehydrogenation temperature was reduced considerably, there is still a big gap in the practical application. ZHANG et al [24] prepared TiO₂ with highly active {001} surface nanosheet catalysts by controlling the crystal surface of TiO₂. With highly active {001} facets, anatase TiO₂ effectively reduced the activation energy of hydrogen desorption. The starting hydrogen release temperature of MgH₂+5wt.%TiO₂ NS was

decreased to 180.5 °C. YIN et al [25] improved the catalytic performance of TiO₂ through multivalent synergistic interactions. They synthesized Ti³⁺ self-doped 3D TiO₂ hollow nanoboxes (Ti³⁺@TiO₂). Ti3+@TiO2 showed a good catalytic effect on the hydrogen storage of MgH2 because of the rich oxygen vacancies and multivalent states of Ti-containing substances formed in situ. The onset hydrogen release temperature of MgH2+ 5wt.%Ti³⁺@TiO₂-5 was 205.4 °C. At 325 °C, 6.1 wt.% hydrogen could be released in 20 min. REN et al [26] enhanced the catalytic activity of TiO₂ by adding oxygen vacancies to its surface. They synthesized TiO₂ nanosheets using a surfactant self-assembly method and a flower-like MgH₂/TiO₂ heterostructure was formed. As a result, the initial hydrogen release temperature of the MgH₂/TiO₂ heterostructure was shifted to 180 °C.

Metal-organic framework (MOF) materials have recently emerged in hydrogen storage field, presenting excellent catalytic properties [27–29]. MOFs have many advantages such as rich pores, large specific surface area, and multiple metal sites, causing much attention in the realm of hydrogen storage. For instance, SHAO et al [30] prepared a thermally stable Ni MOF and doped it to MgH₂. 300 °C, MgH₂-10/Ni-BTC300 5.14 wt.% hydrogen within 3 min. MA et al [31] manufactured TMA-Fe MOFs doped MgH₂ composites and found that the α -Fe generated during the dehydrogenation disrupted the crystal structure of MgH₂ and reduced the nucleation capacity of Mg, thus enhancing the dehydrogenation kinetics of MgH₂. In addition, combining transition metal oxides with MOF materials is an effective approach. ZHANG et al [32] loaded Nb₂O₅ nanoparticles on MOF, and the synergistic effect of Nb₂O₅ and MOF promoted hydrogen desorption and reduced Mg/MgH₂ agglomeration.

Inspired by above encouraging results, we introduced MIL-100(Fe) onto TiO₂ nanosheets and prepared lamellar TiO₂ nanosheets (NS)@MIL-100(Fe) by a self-assembly method. By introducing Fe elements on the TiO₂ surface, Fe ions proliferate into the bulk of TiO₂ NS and remain in the 3⁺ valence state as acceptor-type substituents of Ti⁴⁺, leading to a change in the electron density distribution, which in turn leads to the generation of oxygen vacancies. The presence of oxygen vacancies in the re/dehydrogenation process of

 MgH_2 greatly enhanced the kinetic properties of MgH_2 . At last, the catalytic effect of TiO_2 NS@MIL-100(Fe) on MgH_2 was systematically tested and the catalytic mechanism was elaborated in detail.

2 Experimental

2.1 Chemicals

Tetrabutyl titanate (Ti(OBu)₄, GC, \geq 99.0%) and trimesic acid (benzene-1,3,5-tricarboxylic acid) were purchased from Sinopharm Chemical Reagent. Hydrofluoric acid (HF, GC, \geq 99.99%) and iron(III) nitrate nonahydrate (Fe(NO₃)₃·9H₂O) were purchased from Macklin Corp.

2.2 Preparation of TiO₂ NS

TiO₂ NS was prepared according to a reference [24]. In brief, 5 mL HF and 25 mL Ti(OBu)₄ were mixed in a 100 mL Teflon-lined autoclave and kept at 200 °C for 20 h. After naturally cooling to room temperature, the precipitate was centrifuged and washed thrice with deionized water and ethanol. Finally, the product was collected and dried under vacuum at 80 °C for 6 h.

2.3 Synthesis of TiO₂ NS@MIL-100(Fe)

The three-step preparation of TiO₂ NS@MIL-100(Fe) is illustrated in Fig. 1: (1) assimilation of Fe ions on TiO₂ NS, (2) in situ generation of MIL-100(Fe) on TiO2 NS, and (3) formation of TiO₂ NS@MIL-100(Fe) nanocomposites. Specially, 0.5 g pure TiO₂ NS and 0.808 g Fe(NO₃)₃·9H₂O were dispersed in 50 mL deionized water under sonication for 30 min, and then the solution was stirred for 2 h at 95 °C at a rotation speed of 1200 r/min. Centrifugation with deionized water was performed for 5 times. 10 mmol/L benzene-1,3,5-tricarboxylic acid was added to the centrifuged product in a 100 mL Teflon highpressure reaction liner, and heated at 150 °C for 12 h. Finally, the reaction products were obtained after centrifugation (5 times with deionized water) and vacuum drying.

2.4 Sample characterizations

X-ray diffractometry (XRD) measurements (Rigaku, 40 kV, 40 mA) were performed with a scanning rate of 10 (°)/min from 5° to 80°. The microscopic morphology and elemental distribution

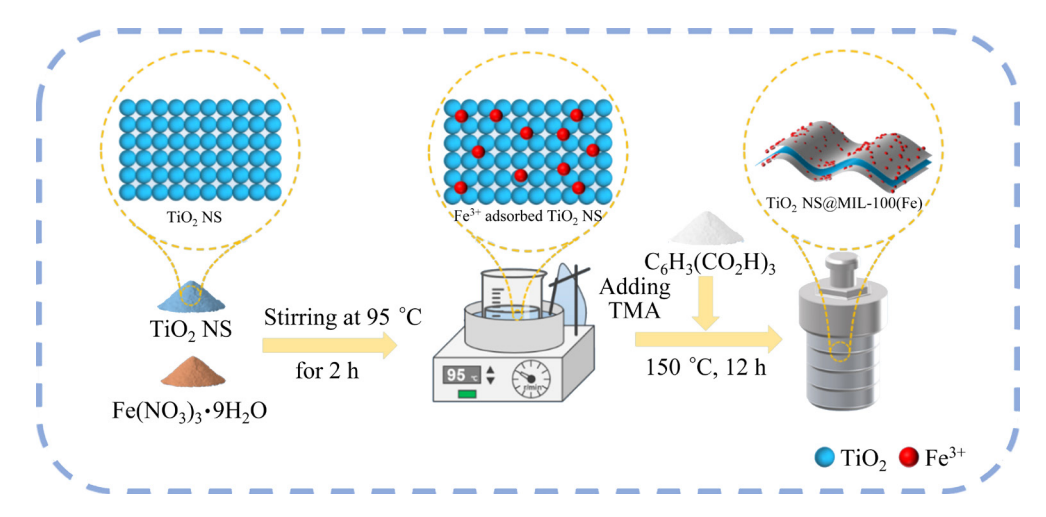


Fig. 1 Schematic diagram for preparation of TiO₂ NS@MIL-100(Fe)

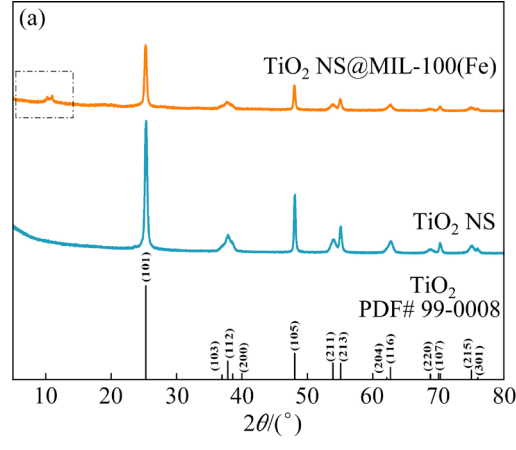
of the samples were analyzed by transmission electron microscopy (TEM, Tecnai G2 F30) and energy dispersive X-ray spectroscopy (EDX). The hydrogen storage properties of the samples were analyzed using a Sieverts-type device designed and assembled in the laboratory. The non-isothermal decomposition experiment was started at room temperature with a heating rate of 5 °C/min, and finished at 450 °C. The isothermal decomposition experiments were performed at 3 MPa H₂ with a fast temperature rise to the desired temperatures. The isothermal hydrogen absorption experiment was performed at a rate of 1°C/min from room temperature to 400 °C under 3 MPa.

3 Results and discussion

3.1 Microstructure of TiO₂ NS@MIL-100(Fe)

To analyze the microstructure of the as-synthesized TiO_2 NS@MIL-100(Fe), XRD measurements were carried out and the results are presented in Fig. 2(a). The diffraction peaks of TiO_2 NS@MIL-100(Fe) at 2θ =25.30°, 37.79°, 48.03°, 55.05° can be attributed to the (101), (004), (200), (211) planes of TiO_2 . To verify the existence of MIL-100(Fe), the selected part in Fig. 2(a) was enlarged. Figure 2(b) shows that the diffraction peaks of 2θ =5°-15° match well with the XRD standard card of #7102029 (MIL-100(Fe)).

TEM characterizations were employed to analyze the microscopic morphology of TiO₂ NS@MIL-100(Fe) and the results are displayed in Figs. 3(a, b). It can be observed that TiO₂ NS@MIL-100(Fe) has an ultrathin lamellar structure



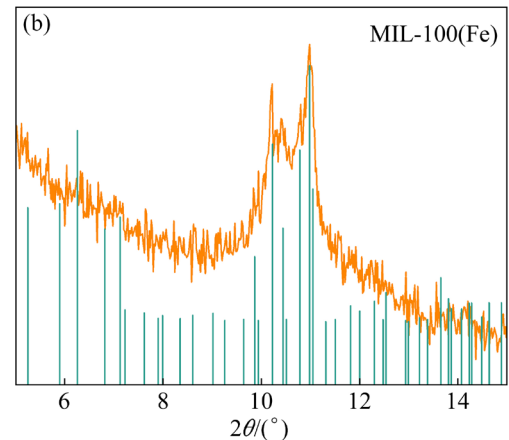


Fig. 2 XRD patterns of TiO₂ NS and TiO₂ NS@MIL-100(Fe) (a), and enlarged selected part (b)

with a thickness of 10 nm and a width of 40 nm. Selected-area electron diffraction rings (Fig. 3(c)) show the (101) and (103) planes of TiO₂, which agree well with the XRD results. The lattice widths of 0.233 nm and 0.243 nm from the n1 and n2 regions in Figs. 3(d, e) are attributed to the (112)

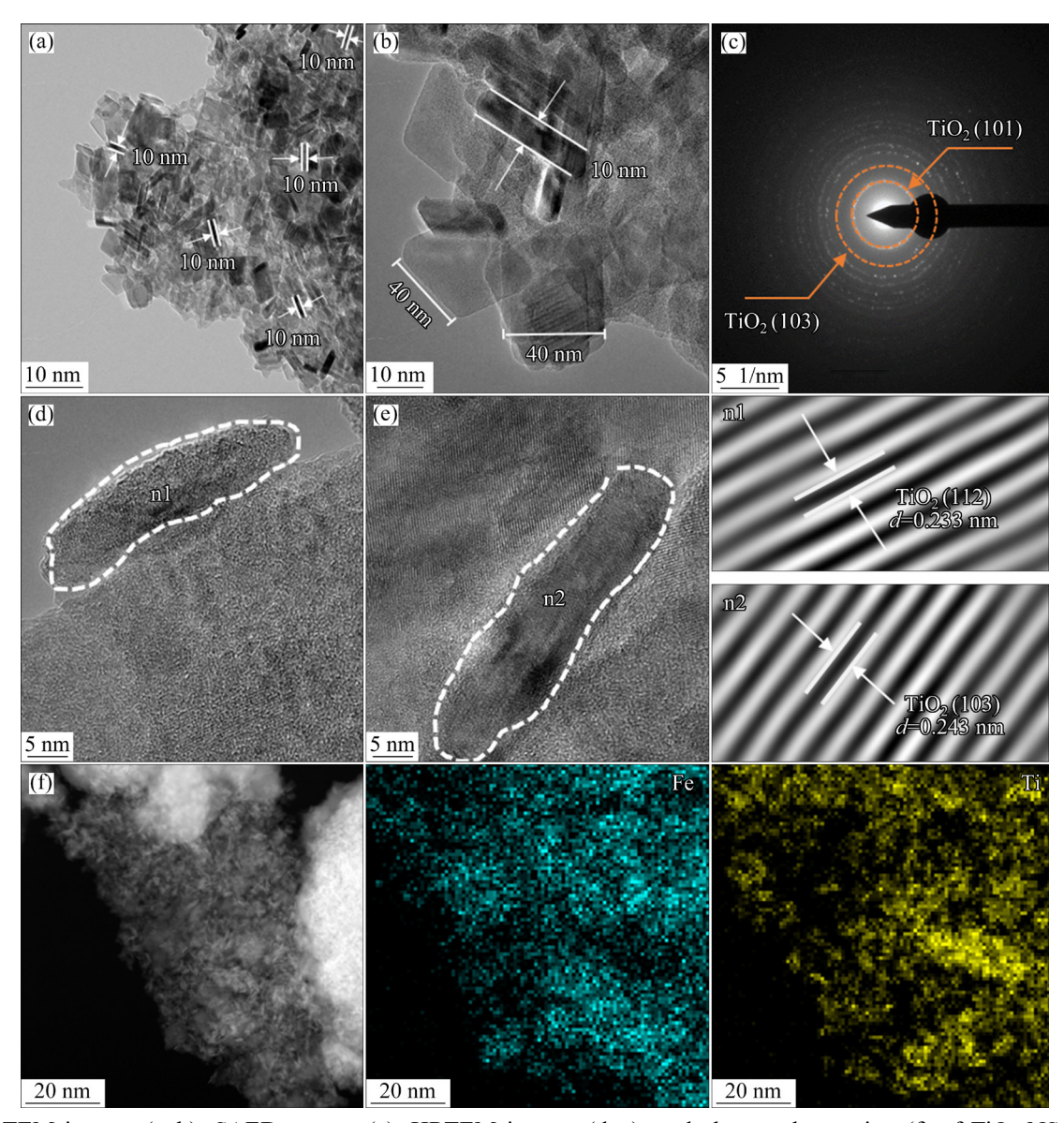


Fig. 3 TEM images (a, b), SAED pattern (c), HRTEM images (d, e), and elemental mapping (f) of TiO₂ NS@MIL-100(Fe) (n1 and n2 are corresponding enlarged regions from (d) and (e))

and (103) planes of TiO_2 , respectively. The EDX spectrum (Fig. 3(f)) shows that the Fe element is evenly distributed on the surface of TiO_2 , demonstrating successful loading of MIL-100(Fe) on TiO_2 NS.

3.2 Hydrogen storage performance of MgH₂+ TiO₂ NS@MIL-100(Fe) composites

To investigate the catalytic effect of TiO₂ NS@MIL-100(Fe) on MgH₂, a dehydrogenation test of MgH₂ with different catalysts was conducted, as illustrated in Fig. 4(a). The dehydrogenation temperature of the MgH₂+7wt.%TiO₂ NS is 210 °C, 140 °C lower than that of pristine MgH₂. With the loading of MIL-100(Fe) on TiO₂ NS, the initial

dehydrogenation temperature of MgH₂+7wt.%TiO₂ NS@MIL-100(Fe) is further reduced to 200 °C. Besides, the composite can discharge 6.2 wt.% H₂ below 300 °C in the non-isothermal dehydrogenation test, while MgH₂+7wt.%TiO₂ NS only desorbs 5.8 wt.% H₂. Figure 4(b) compares the starting dehydrogenation temperature of MgH₂ with the addition of TiO₂-based and Fe-based catalysts. Clearly, TiO₂ NS@MIL-100(Fe) presents the lowest on-set dehydrogenation temperature, so the subsequent experiments were mainly carried out on TiO₂ NS@MIL-100(Fe).

An experimental study on the isothermal dehydrogenation of $MgH_2+7wt\%TiO_2$ NS@MIL-100(Fe) and MgH_2 at different temperatures is

presented in Figs. 4(c, d). At the temperature of 235 °C, MgH₂+7wt.%TiO₂ NS@MIL-100(Fe) can release 4.71 wt.% H₂ within 20 min. In comparison, even at a much higher temperature of 335 °C, MgH₂ only desorbs 2.71 wt.% H₂ in 20 min. Although the temperature of MgH₂+7wt.%TiO₂ NS@MIL-100(Fe) is 100 °C lower than that of MgH₂, the hydrogen desorption rate is 1.7 times faster than

that of MgH₂. Increasing the temperature to 250 °C, MgH₂+7wt.%TiO₂ NS@MIL-100(Fe) releases 6 wt.% H₂ within 10 min. Additionally, TiO₂ NS@ MIL-100(Fe) exhibits superior isothermal hydrogen desorption performance compared to other TiO₂-based and Fe-based catalysts (Table 1). In summary, TiO₂ NS@MIL-100(Fe) has a significant catalytic effect on the dehydrogenation kinetics of MgH₂.

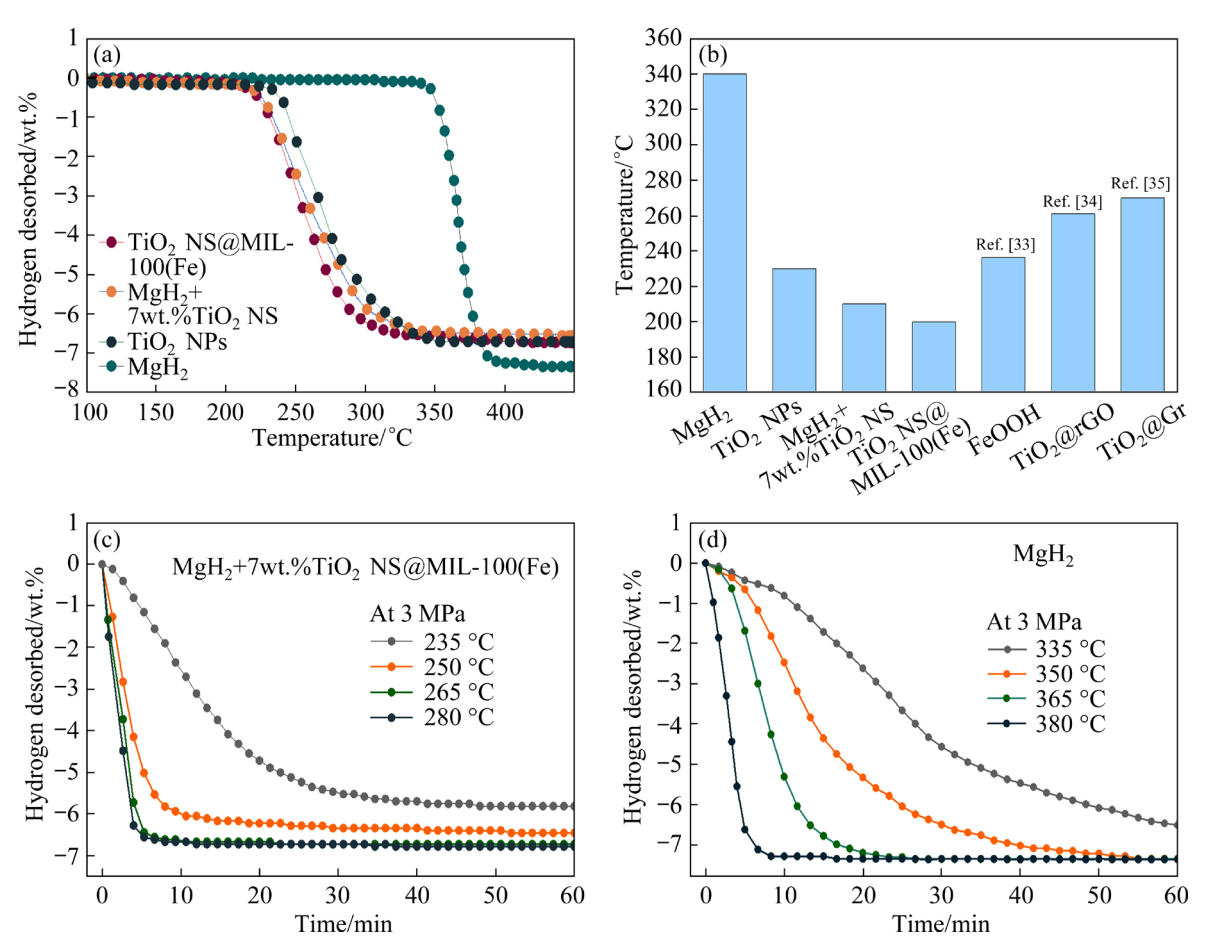


Fig. 4 Non-isothermal dehydrogenation of MgH₂, MgH₂+7wt.%TiO₂ NS, TiO₂ NPs, TiO₂ NS@MIL-100(Fe) (a); Comparison of dehydrogenation temperatures (b); Isothermal dehydrogenation curves of MgH₂+7wt.%TiO₂ NS@MIL-100(Fe) (c) and MgH₂ (d)

Table 1 Comparison of dehydrogenation performance for Mg-based composites

Sample	Isothermal dehydrogenation performance			Source
	Dehydrogenation content/wt.%	Reaction temperature/°C	Reaction time/min	Source
MgH ₂ -Fe NS	2.4	275	60	Ref. [36]
MgH ₂ -Ni/TiO ₂	5.2	250	20	Ref. [37]
MgH ₂ -3DOM TiO ₂	5.7	275	50	Ref. [38]
MgH ₂ -(Ni-TiO ₂)/rGO	4.3	250	30	Ref. [39]
MgH_2 - TiO_2 @ C	5.9	250	20	Ref. [40]
$MgH_2Ti^{3+} @TiO_2$	1.2	250	120	Ref. [25]
MgH ₂ -TiO ₂ NS@MIL-100(Fe)	6.0	250	10	This work

Subsequently, non-isothermal and isothermal hydrogenation tests were performed on the dehydrogenated samples. As shown in Fig. 5(a), MgH₂+7wt.%TiO₂ NS@MIL-100(Fe) starts to absorb hydrogen at room temperature (25 °C), achieving dramatical reduction at 100 °C compared to MgH₂. When the temperature is raised to 200 °C, MgH₂+7wt.%TiO₂ NS@MIL-100(Fe) absorbs 6.7 wt.% H₂, whereas MgH₂ only uptakes 2.3 wt.% H₂. Additionally, 3 wt.% H₂ can be absorbed by MgH₂+7wt.%TiO₂ NS@MIL-100(Fe) at 100 °C within 25 min (Fig. 5(b)) while 45 min is required for MgH₂ even at a higher temperature of 200 °C

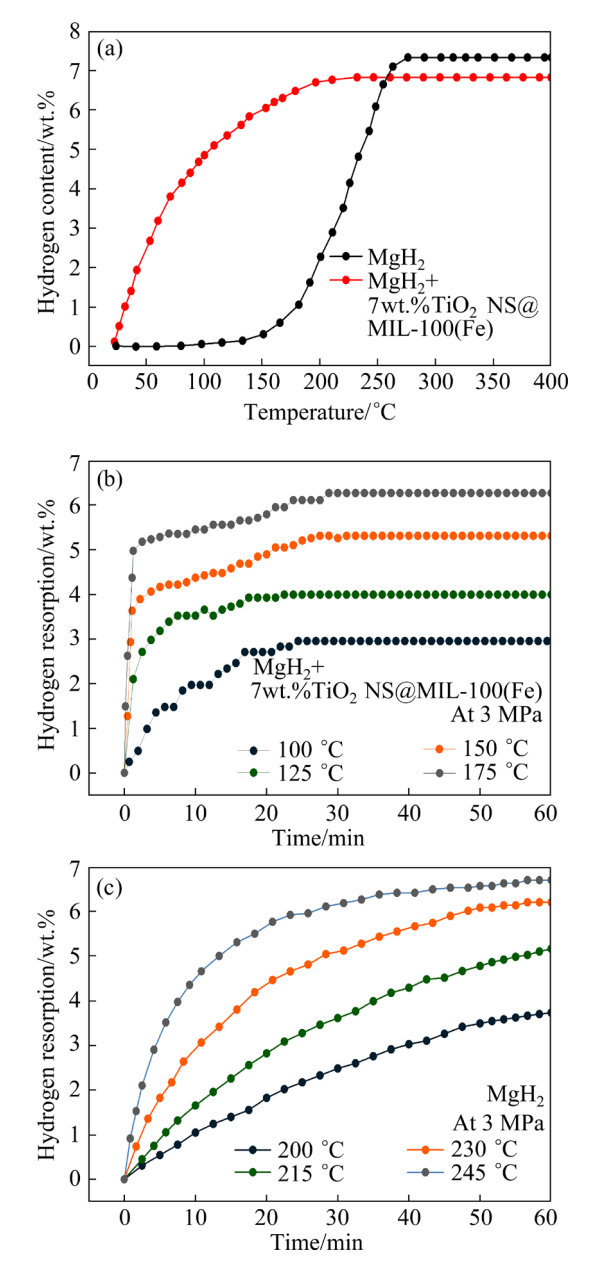


Fig. 5 Non-isothermal (a) and isothermal hydrogenation curves of $MgH_2+7wt.\%TiO_2$ NS@MIL-100(Fe) (b) and MgH_2 (c)

(Fig. 5(c)). Apparently, TiO₂ NS@MIL-100(Fe) has a significant promotion effect on the hydrogen absorption kinetics of MgH₂.

To elaborate more deeply on the enhancement of the kinetics of MgH₂–TiO₂ NS@MIL-100(Fe) composites, Johnson–Mehl–Avrami–Kolmogorov (JMAK) equation [41] was used to calculate the de/rehydrogenation apparent activation energy (E_a). Calculated results show that the dehydrogenation and hydrogenation activation energies of MgH₂+7wt.%TiO₂ NS@MIL-100(Fe) are 70.62 and 70.70, 88.2 and 16.3 kJ/mol lower than those of MgH₂ (Fig. 6), respectively. The above results indicate that the activation energy of MgH₂ can be effectively reduced by adding TiO₂ NS@MIL-100(Fe), contributing to the superior kinetic properties of MgH₂+7wt.%TiO₂ NS@MIL-100(Fe).

Cycling performance is a prominent criterion for evaluating the hydrogen storage capacity of the composite. For this reason, 50 cycles of MgH₂+7wt.%TiO₂ NS@MIL-100(Fe) were performed at 300 °C. The results are presented in Fig. 7. Although the hydrogen storage performance declines in cycling, the hydrogen storage capacity of the sample

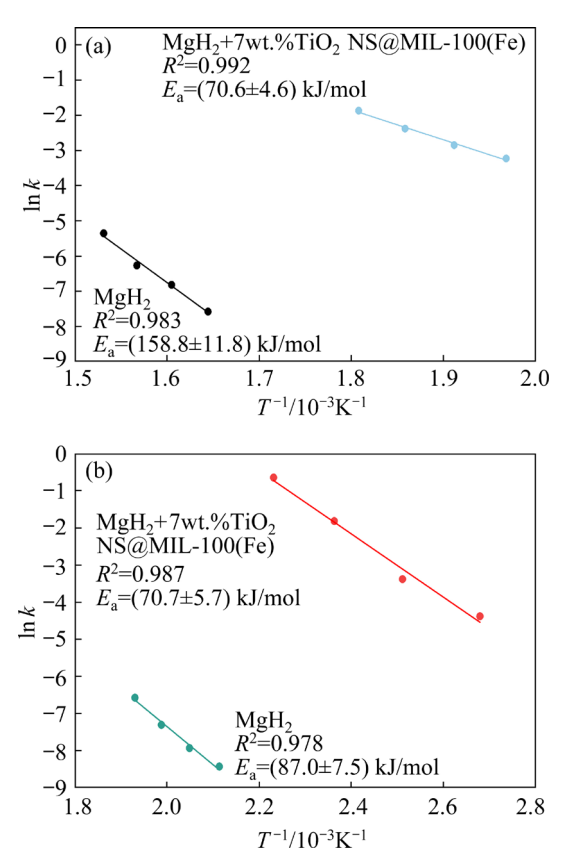


Fig. 6 Dehydrogenation (a) and rehydrogenation (b) activation energy of MgH_2 and $MgH_2+7wt.\%TiO_2$ NS@ MIL-100(Fe)

is recovered in the 50 h cycle by increasing the hydrogen pressure to 5 MPa. In the 50th cycle, 6.62 wt.% of H₂ is released, achieving only 0.28 wt.% decrease in capacity compared with the first cycle. The reason for the decrease in reversible hydrogen storage capacity is that nanoscale MgH₂ is highly susceptible to particle aggregation and growth during hydrogen absorption and desorption, thus causing capacity decay and kinetic degradation.

3.3 Catalytic mechanism

The XRD tests were utilized to analyze the phase changes on the de/rehydrogenated samples. The peak of MgO in Fig. 8 is possibly caused by oxygen contamination during or before the XRD sample testing. The XRD data indicate that interconversion between Mg and MgH₂ mainly occurs during de/rehydrogenation processes. As TiO₂ and MgH₂ peaks are very close to each other, TEM and XPS measurements were adopted to analyze the samples.

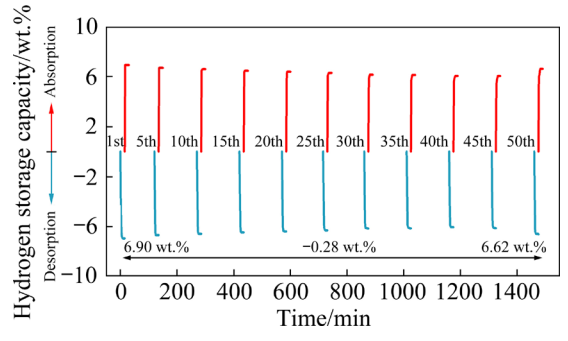


Fig. 7 Isothermal dehydrogenation/hydrogenation curves of MgH₂+7wt.%TiO₂ NS@MIL-100(Fe) composite at 300 °C for 50 cycles

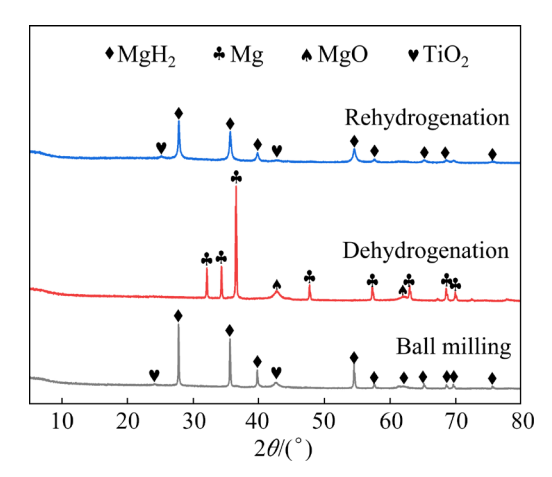


Fig. 8 XRD patterns for MgH $_2$ +7wt.%TiO $_2$ NS@ MIL-100(Fe) in ball-milling, rehydrogenation, and dehydrogenation processes

According to Figs. 9(a, b), the XPS survey spectrum shows that TiO₂@MIL-100(Fe) contains Ti, O, Fe and C elements and TiO₂ NS has elements of Ti and O. The high-resolution spectrum of O 1s in TiO₂@MIL-100(Fe) (Fig. 9(c)) consists of three peaks at 531.4, 530.4 and 528.8 eV [42]. XPS profile in Fig. 9(d) presents that the dominant peaks centered at 724.3 and 709.8 eV correspond to Fe $2p_{1/2}$ and Fe $2p_{3/2}$ of TiO₂NS@MIL-100(Fe), respectively. Notably, it can be observed that the dominant peaks shift negatively compared with the standard peaks of Fe³⁺ (blue line in Fig. 9(d)) [43], which suggests that the Fe - O - Ti bond is generated at the interface of MIL-100(Fe) and TiO₂ [42]. Moreover, the peaks at 463.6 and 458.5 eV belong to Ti 2p_{1/2} and Ti 2p_{3/2}, respectively (Figs. 9(e, g)). Because of the presence of the Fe—O—Ti bond in TiO₂@MIL-100(Fe), the density of the electron cloud outside the Ti ion is increased, resulting a shift in the peaks [26,42]. Therefore, with the growth of MIL-100(Fe) on the surface of TiO₂ NS, some Fe atoms substitute for Ti atoms to produce Fe-O-Ti bonds, contributing to the creation of rich oxygen vacancies on the TiO2 surface [44].

To ensure that the valence and bonding of Ti could be effectively determined in the composites, the doping content of TiO₂ NS@MIL-100(Fe) to MgH₂ was increased to 20 wt.%. The highresolution Ti 2p XPS spectra (Figs. 9(f, h)) show that the Ti⁴⁺ signal can be detected for the samples in different states (458.9 eV for 2p_{3/2}, and 464.6 eV for $2p_{1/2}$), which confirms the presence of TiO₂ in the de/rehydrogenation samples. Meanwhile, the signals of Ti^{3+} (456.7 eV for $2p_{3/2}$ and 462.4 eV for 2p_{1/2}) are observed in both hydrogen-charged and discharged states, proving the existence of oxygen vacancies in both states. Oxygen vacancies not only accelerate the diffusion of hydrogen atoms and electron migration, but also create more active sites for the absorption of hydrogen and the nucleation of Mg/MgH₂ [26]. In addition, the position of the central peak of Ti2+ in the hydrogen-discharged state negatively shifts compared to that of the hydrogen-charged state. The presence of Ti²⁺ proves the creation of a low-valent Ti - H active component, which can contribute to the transport of hydrogen and the transfer of electrons, thus decreasing the potential barrier for the binding of hydrogen atoms on the surface of MgH₂ [45,46]. It

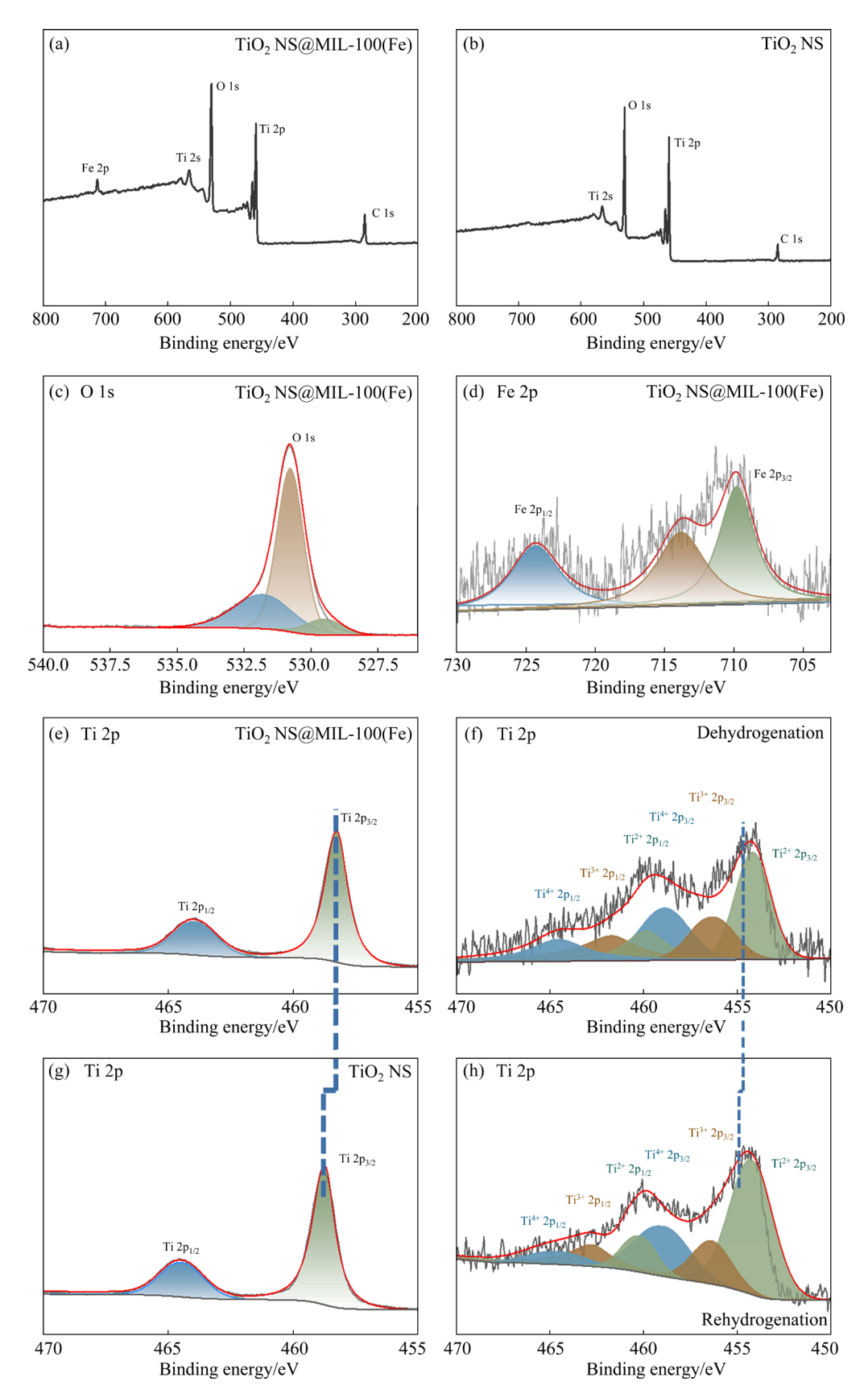


Fig. 9 XPS spectra of TiO₂ NS@MIL-100(Fe) (a) and TiO₂ NS (b); O 1s (c) and Fe 2p (d) XPS spectra of TiO₂ NS@MIL-100(Fe); Ti 2p XPS spectra of TiO₂ NS@MIL-100(Fe) (e) and TiO₂ NS (g); Ti 2p XPS spectra of MgH₂+ 20wt.%TiO₂ NS@MIL-100(Fe) after dehydrogenation (f) and rehydrogenation (h)

is known that the electronegativity of Ti (1.54) is located between Mg (1.31) and H (2.2) [47,48]. The change of valence state of Ti facilitates the transfer of electrons between Mg²⁺ and H⁻, providing beneficial conditions for the weakening of Mg—H bonds. Based on the above, the production of multivalent Ti greatly improves the dynamics of MgH₂.

The ball-milled samples were analyzed by TEM to determine their material composition and morphological structure. It can be observed in Figs. 10(a-c) that TiO₂ NS@MIL-100(Fe) changes from nanosheets into nanowires after ball milling with MgH₂. Selected electron diffraction rings (Fig. 10(d)) exhibit the (213) and (119) planes of TiO₂ and the (202) and (111) planes of MgH₂. The lattice spacings of 0.219 and 0.243 nm for the selected m1 and n1 regions in Fig. 10(e) correspond to the (111) plane of MgH₂ and the (103) plane of TiO₂, respectively. Similarly, the selected m2 and n2 regions in Fig. 10(f) have lattice spacings of 0.251 and 0.350 nm, corresponding to the (101) plane of MgH₂ and TiO₂, respectively. The TEM results of the ball-milled samples are consistent with XRD results. EDX exhibits essentially the same distribution of Fe and Ti elements with Mg elements (Fig. 10(g)), confirming the homogeneous distribution of TiO₂ NS@MIL-100 (Fe) over MgH₂. The uniform distribution of TiO₂ NS@MIL-100(Fe) over MgH₂ surfaces is conducive to enlarging the contact area between TiO₂ NS@MIL-100(Fe) and MgH₂, thus providing more nucleation sites and facilitating the transport and diffusion of H₂.

By combining XRD, XPS, and TEM analyses, the following conclusions can be obtained. After ball milling with MgH₂, TiO₂ NS@MIL-100(Fe) is fragmented into even finer nanowires and uniformly anchored on the surface of the MgH₂ particles, enlarging the contact area and creating a large number of nucleation sites and diffusion channels for the catalysis of the solid-state de/rehydrogenation reaction. On the one hand, oxygen vacancies are created due to the partial replacement of Ti atoms by Fe atoms during the growth of MIL-100(Fe) on the TiO₂ NS surface. The presence of oxygen vacancies greatly improve the electron migration rate, which is beneficial for exerting robust catalytic action. On the other hand,

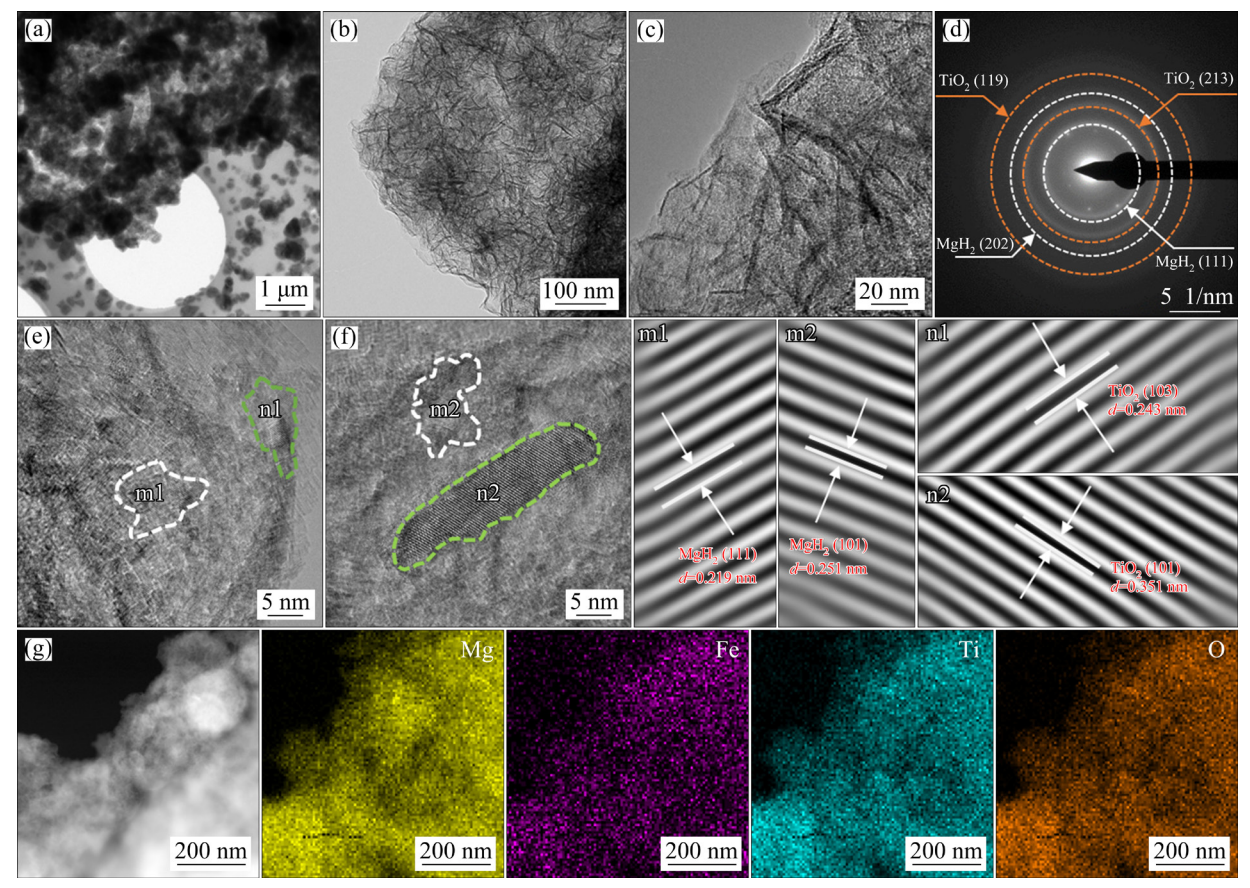


Fig. 10 TEM images (a-c), SAED pattern (d), HRTEM images (e, f), and elemental mapping (g) of MgH₂+7wt.%TiO₂ NS@MIL-100(Fe) (m1, m2, n1 and n2 are the corresponding enlarged regions in (e, f))

the creation of multivalent states during hydrogen absorption and desorption provides favorable conditions for weakening the Mg—H bond and reducing the binding barrier for H atoms. Therefore, TiO₂ NS@MIL-100(Fe) presents excellent catalytic efficacy for magnesium-based hydrogen storage materials.

4 Conclusions

- (1) Lamellar TiO_2 NS@MIL-100(Fe) is successfully synthesized by a self-assembly method. TiO_2 NS@MIL-100(Fe) significantly enhances the hydrogen storage properties of MgH₂.
- (2) MgH₂+7wt.%TiO₂ NS@MIL-100(Fe) starts to release hydrogen at 200 °C. At 235 °C, 4.71 wt.% H₂ was released in 20 min. Besides, the activation energy of dehydrogenation of MgH₂+7wt.%TiO₂ NS@MIL-100(Fe) is reduced to 70.62 kJ/mol. Moreover, MgH₂+7wt.%TiO₂ NS@MIL-100(Fe) still retains 6.62 wt.% hydrogen storage capacity after 50 cycles, showing excellent cycling performance.
- (3) The oxygen-rich vacancies and multivalent Ti environment synergistically contribute to the improvement in the hydrogen storage performance of MgH₂. This study provides an efficient and simple method for synthesizing TiO₂ with rich oxygen vacancies and demonstrates a feasible solution to promote the hydrogen storage performance of MgH₂.

CRediT authorship contribution statement

Ren ZHOU: Investigation, Formal analysis, Writing – Review & editing; Li WANG: Validation; Tao ZHONG: Formal analysis; Shuai LI: Investigation; Dong-qiang GAO: Investigation; Fu-ying WU: Supervision, Resources; Liu-ting ZHANG: Supervision, Resources, Writing – Review & editing.

Declaration of competing interest

The authors declare that they have no known competing financial interests or personal relationships that could have appeared to influence the work reported in this paper.

Acknowledgments

The authors are grateful for the financial support from the National Natural Science Foundation of China (No. 51801078).

References

- [1] XIA Guang-lin, TAN Ying-bin, CHEN Xiao-wei, SUN Da-lin, GUO Zai-ping, LIU Hua-kun, OUYANG Liu-zhang, ZHU Min, YU Xue-bin. Monodisperse magnesium hydride nanoparticles uniformly self-assembled on graphene [J]. Advanced Materials, 2015, 21: 5981–5988.
- [2] LI Shuai, ZHANG Liu-ting, WU Fu-ying, JIANG Yi-qun, YU Xue-bin. Efficient catalysis of FeNiCu-based multi-site alloys on magnesium-hydride for solid-state hydrogen storage [J]. Chinese Chemical Letters, 2024: 109566.
- [3] ZHANG Chun-min, LIANG Long, ZHAO Shao-lei, WU Zhi-jian, WANG Shao-hua, YIN Dong-ming, WANG Qing-shuang, WANG Li-min, WANG Chun-li, CHENG Yong. Dehydrogenation behavior and mechanism of LiAlH₄ adding nano-CeO₂ with different morphologies [J]. Nano Research, 2023, 16: 9426–9434.
- [4] LU Xiong, ZHANG Liu-ting, YU Hai-jie, LU Zhi-yu, HE Jia-huan, ZHENG Jia-guang, WU Fu-ying, CHEN Li-xin. Achieving superior hydrogen storage properties of MgH₂ by the effect of TiFe and carbon nanotubes [J]. Chemical Engineering Journal, 2021, 422: 130101.
- [5] LIANG Long, ZHAO Shao-lei, WANG Chun-li, YIN Dong-ming, WANG Shao-hua, WANG Qing-shuang, LIANG Fei, LI Shou-liang, WANG Li-min, CHENG Yong. Heterojunction synergistic catalysis of MXene-supported PrF₃ nanosheets for the efficient hydrogen storage of AlH₃ [J]. Nano Research, 2023, 16: 9546–9552.
- [6] ZHANG Jian, HE Liu, YAO Yuan, ZHOU Xiao-jie, JIANG Li-lun, PENG Ping, Hydrogen storage properties of magnesium hydride catalyzed by Ni-based solid solutions [J]. Transactions of Nonferrous Metals Society of China, 2022, 32: 604–617.
- [7] YANG Zheng-xuan, LI Xiu-gang, YAO Qi-lu, LU Zhang-hui, ZHANG Ning, YANG Kai, WANG Yu-qing, ZHANG Kan, LIU Hai-zhen, ZHANG Liu-ting, LIN Huai-jun, ZHOU Qing-jun, WANG Fang, YU Zhi-ming, MA Jian-min. Roadmap on hydrogen energy from production to utilizations [J]. Rare Metals, 2022, 41: 3251–3267.
- [8] ZHONG Tao, ZHANG Hao-yu, SONG Meng-chen, JIANG Yi-qun, SHANG Dan-hong, WU Fu-ying, ZHANG Liu-ting. FeCoNiCrMo high entropy alloy nanosheets catalyzed magnesium hydride for solid-state hydrogen storage [J]. International Journal of Minerals, Metallurgy and Materials, 2023, 30: 2270–2279.
- [9] ZHANG Hao-yu, TIAN Gui-bin, WU Fu-ying, YAO Zhen-dong, ZHENG Jia-guang, ZHANG Liu-ting. Catalytic effect of two-dimensional Mo₂TiC₂ MXene for tailoring hydrogen storage performance of MgH₂ [J]. Transactions of Nonferrous Metals Society of China, 2023, 33: 3465–3475.
- [10] CHEN Yan, ZHANG Hao-yu, WU Fu-ying, SUN Ze, ZHENG Jia-guang, ZHANG Liu-ting, CHEN Li-xin. Mn nanoparticles enhanced dehydrogenation and hydrogenation kinetics of MgH₂ for hydrogen storage [J]. Transactions of Nonferrous Metals Society of China, 2021, 31: 3469–3477.
- [11] LU Zi-chuan, LI Shuai, ZHAO Chang-hao, ZHENG Jia-guang, SHANG Dan-dong, WU Fu-ying, ZHANG Liuting. Schottky-structured CoNi-CoO@rGO for accelerating hydrogen storage in magnesium hydride [J]. Journal of

- Alloys and Compounds, 2024, 970: 172715.
- [12] NORBERG N S, ARTHUR T S, FREDRICK S J, PRIETO A L. Size-dependent hydrogen storage properties of Mg nanocrystals prepared from solution [J]. Journal of the American Chemical Society, 2011, 133: 10679–10681.
- [13] ZHOU Cai-qin, PENG Ya-yu, ZHANG Qin-gan. Growth kinetics of MgH₂ nanocrystallites prepared by ball milling [J]. Journal of Materials Science & Technology, 2020, 50: 178–183.
- [14] SHEN Hao, JIANG Li-jun, LI Ping, YUAN Hui-ping, LI Zhi-nian, ZHANG Jun-xian. Heat treatment effect on structural evolution and hydrogen sorption properties of Y_{0.5}La_{0.2}Mg_{0.3-x}Ni₂ compound [J], Rare Metals, 2023, 42: 1813–1820.
- [15] YANG Yan, XIONG Xiao-ming, CHEN Jing, PENG Xiao-dong, CHEN Dao-lun, PAN Fu-sheng. Research advances of magnesium and magnesium alloys worldwide in 2022 [J]. Journal of Magnesium and Alloys, 2023. 11: 2611–2654.
- [16] ZHANG Wei, ZHAO Dong-liang, ZHANG Yang-huan, GUO Shi-hai, QI Yan. Microstructure and hydrogen storage property of as-milled La-Y-Mg-Ni alloy [J]. Transactions of Nonferrous Metals Society of China, 2023, 33: 3783-3796.
- [17] GAO Dong-qiang, ZHANG Liu-ting, SONG Meng-chen, WU Fu-ying, WANG Jiao, ZHAO Hu, LI Hong. Interfacial engineering of nickel/vanadium based two-dimensional layered double hydroxide for solid-state hydrogen storage in MgH₂ [J]. International Journal of Hydrogen Energy, 2023, 48: 9390–9400.
- [18] WANG Li, ZHANG Liu-ting, LU Xiong, WU Fu-ying, SUN Ze, ZHAO Hu, LI Hong. Surprising cocktail effect in high entropy alloys on catalyzing magnesium hydride for solid-state hydrogen storage [J]. Chemical Engineering Journal, 2023, 465: 142766.
- [19] LI Shuai, WU Fu-ying, ZHANG Yan, ZHOU Ren, LU Zi-chuan, JIANG Yi-qun, BIAN Ting, SHANG Dan-hong, ZHANG Liu-ting. Enhanced hydrogen storage performance of magnesium hydride catalyzed by medium-entropy alloy CrCoNi nanosheets [J]. International Journal of Hydrogen Energy, 2024, 50: 1015–1024.
- [20] SHI Qing-yun, GAO Yu-xing, ZHAO Shao-lei, ZHANG Chun-min, LIU Cong, WANG Chun-li, WANG Shao-hua. Interfacial engineering of fluorinated TiO₂ nanosheets with abundant oxygen vacancies for boosting the hydrogen storage performance of MgH₂ [J]. Small, 2023: 2307965.
- [21] CHEN Man, XIAO Xue-zhang, ZHANG Meng, ZHENG Jia-guang, Liu Me-jia, WANG Xuan-cheng, JIANG Li-jun, CHEN Li-xin. Highly dispersed metal nanoparticles on TiO₂ acted as nano redox reactor and its synergistic catalysis on the hydrogen storage properties of magnesium hydride [J]. International Journal of Hydrogen Energy, 2019, 44: 15100–15109.
- [22] Duan Xing-qing, LI Guang-xu, ZHANG Wen-hui, LUO Hui, TANG Hai-mei, LI Xu, Peng Sheng. Ti₃AlCN MAX for tailoring MgH₂ hydrogen storage material: From performance to mechanism [J]. Rare Metals, 2023, 42: 1923–1934.
- [23] CROSTON D L, GRANT D M, WALKER G S. The catalytic effect of titanium oxide based additives on the

- dehydrogenation and hydrogenation of milled MgH₂ [J]. Journal of Alloys and Compounds, 2010, 492: 251–258.
- [24] MA Zhong-liang, LIU Jiang-chuan, ZHU Yun-feng, ZHAO Ying-yan, LIN Huai-jun, ZHANG Yao, LI Hai-wen, ZHANG Ji-guang, LIU Yang, GAO Wen-tian, LI Shan-shan, LI Li-quan. Crystal-facet-dependent catalysis of anatase TiO₂ on hydrogen storage of MgH₂ [J]. Journal of Alloys and Compounds, 2020, 822: 153553.
- [25] YIN Cheng-wang, QIU Shu-jun, WANG Yu-huan, WEI Qiu-hong, PENG Zhi-wei, XIA Yong-peng, ZOU Yong-jin, XU Fen, Sun Li-xian, CHU Hai-liang. Promoted hydrogen storage properties of MgH₂ by Ti³⁺ self-doped defect-mediated TiO₂ [J]. Journal of Alloys and Compounds, 2023, 966: 171610.
- [26] REN Li, ZHU Wen, LI Ying-hui, LIN Xi, XU Hao, SUN Feng-zhan, LU Chong, ZOU Jian-xin. Oxygen vacancy-rich 2D TiO₂ nanosheets: A bridge toward high stability and rapid hydrogen storage kinetics of nano-confined MgH₂ [J]. Nano-Micro Letters, 2022, 14: 144.
- [27] YANG Hui-min, LIU Xian, SONG Xiu-li, YANG Tai-lai, LIANG Zhen-hai, FAN Cai-mei. In situ electrochemical synthesis of MOF-5 and its application in improving photocatalytic activity of BiOBr [J]. Transactions of Nonferrous Metals Society of China, 2015, 25: 3987–3994.
- [28] LI Zeng-yi, SUN Li-xian, XU Fen, LUO Yu-mei, XIA Yong-peng, WEI Sheng, ZHANG Cheng-cheng, CHENG Ri-guang, YE Chao-feng, LIU Meng-yuan, ZENG Ju-lan, CAO Zhong, PAN Hong-ge. Modulated noble metal/2D MOF heterostructures for improved hydrogen storage of MgH₂ [J]. Rare Metals, 2024, 43: 1672–1685.
- [29] GAO Hai-guang, SHI Rui, SHAO Yu-ting, LIU Yang, ZHU Yun-feng, ZHANG Ji-guang, LI Li-quan. Catalysis derived from flower-like Ni MOF towards the hydrogen storage performance of magnesium hydride [J]. International Journal of Hydrogen Energy, 2022, 47: 9346–9356.
- [30] SHAO Hu-xu, HUANG Yi-ke, GUO Hui-nan, LIU Ya-fei, GUO Yu-sang, WANG Yi-jing. Thermally stable Ni MOF catalyzed MgH₂ for hydrogen storage [J]. International Journal of Hydrogen Energy, 2021, 46: 37977–37985.
- [31] MA Zhe-wen, ZHANG Qiu-yu, ZHU Wen, KHAN D, HU Chuan-zhu, HUANG Ti-ping, DING Wen-jiang, ZOU Jian-xin. Nano Fe and Mg₂ Ni derived from TMA-TM (TM= Fe, Ni) MOFs as synergetic catalysts for hydrogen storage in MgH₂ [J]. Sustainable Energy & Fuels, 2020, 4: 2192–2200.
- [32] ZHANG Liu-ting, NYAHUMA F M, ZHANG Hao-yu, CHENG Chang-shan, ZHENG Jia-guang, WU Fu-ying, CHEN Li-xin. Metal organic framework supported niobium pentoxide nanoparticles with exceptional catalytic effect on hydrogen storage behavior of MgH₂ [J]. Green Energy & Environment, 2023, 8: 589–600.
- [33] SONG Meng-chen, ZHANG Liu-ting, ZHENG Jia-guang, YU Zi-dong, WANG Sheng-nan. Constructing graphene nanosheet-supported FeOOH nanodots for hydrogen storage of MgH₂ [J]. International Journal of Minerals, Metallurgy and Materials, 2022, 29: 1464–1473.
- [34] LIU Guan-hao, WANG Lu-xiang, HU Yi-wang-ting, SUN Cheng-hua, LENG Hai-yan, LI Qian, WU Cheng-zhang. Enhanced catalytic effect of TiO2@rGO synthesized by one-pot ethylene glycol-assisted solvothermal method for MgH₂ [J]. Journal of Alloys and Compounds, 2021, 881:

160644.

- [35] VERMA S K, BHATNAGAR A, SHUKLA V, SONI P K, PANDEY A P, YADAB T P, SRIVASTAVA O N. Multiple improvements of hydrogen sorption and their mechanism for MgH₂ catalyzed through TiH₂@Gr [J]. International Journal of Hydrogen Energy, 2020, 45: 19516–19530.
- [36] ZHANG Liu-ting, JI Liang, YAO Zhen-dong, YAN Nian-hua, YANG Xing-lin, ZHU Xin-qian, HU Shuang-lin, CHEN Li-xin. Facile synthesized Fe nanosheets as superior active catalyst for hydrogen storage in MgH₂ [J]. International Journal of Hydrogen Energy, 2019, 44: 21955–21964.
- [37] ZHANG Ji-guang, SHI Rui, ZHU Yun-feng, LIU Ya-na, ZHANG Yao, LI Shan-shan, LI Li-qian. Remarkable synergistic catalysis of Ni-doped ultrafine TiO₂ on hydrogen sorption kinetics of MgH₂ [J]. ACS Applied Materials & Interfaces, 2018, 10: 24975–24980.
- [38] SHAO Yu-ting, GAO Hai-guang, TANG Qin-ke, LIU Ya-na, LIU Jiang-chuan, ZHU Yun-feng, ZHANG Ji-guang, LI Li-quan, HU Xiao-hui, BA Zhi-xin. Ultra-fine TiO₂ nanoparticles supported on three-dimensionally ordered macroporous structure for improving the hydrogen storage performance of MgH₂ [J]. Applied Surface Science, 2022, 585: 152561.
- [39] ZENG Liang, QING Pei-lin, CAI Fang-fang, HUANG Xian-tun, LIU Hai-zhen, LAN Zhi-qiang, GUO Jin. Enhanced hydrogen storage properties of MgH₂ using a Ni and TiO₂ co-doped reduced graphene oxide nanocomposite as a catalyst [J]. Frontiers in Chemistry, 2020, 8: 207.
- [40] ZHANG Xin, LENG Zi-han, GAO Ming-xia, HU Jian-jiang, DU Fang, YAO Jiao-hua, Pan Hong-ge, LIU Yong-feng. Enhanced hydrogen storage properties of MgH₂ catalyzed with carbon-supported nanocrystalline TiO₂ [J]. Journal of Power Sources, 2018, 398: 183–192.
- [41] ZHANG Jian, YAN Shuai, XIA Guang-lin, ZHOU Xiao-jie, LU Xian-zheng, YU Lin-ping, YU Xue-bin, PENG Ping. Stabilization of low-valence transition metal towards advanced catalytic effects on the hydrogen storage

- performance of magnesium hydride [J]. Journal of Magnesium and Alloys, 2021, 9: 647–657.
- [42] HE Xiang, FANG Hong, GOSZTOLA D J, JIANG Zhang, JENA P, WANG Wei-ning. Mechanistic insight into photocatalytic pathways of MIL-100(Fe)/TiO₂ composites [J]. ACS Applied Materials & Interfaces, 2019, 11: 12516– 12524.
- [43] DUPIN K C, GONBEAU D, VINATIER P, LEAVASSEUI A. Systematic XPS studies of metal oxides, hydroxides and peroxides [J]. Physical Chemistry Chemical Physics, 2000, 2: 1319–1324.
- [44] REN Li, LI Ying-Hui, LI Zi, LIN Xi, LU Chong, DING Wen-jiang, ZOU Jian-xin. Boosting hydrogen storage performance of MgH₂ by oxygen vacancy-rich H-V₂O₅ nanosheet as an excited H-pump [J], Nano-Micro Letters, 2024, 16: 160.
- [45] PAN Xiao-yang, YANG Min-quan, FU Xian-zhi, ZHANG Nan, XU Yi-jun. Defective TiO₂ with oxygen vacancies: Synthesis, properties and photocatalytic applications [J]. Nanoscale, 2013, 5: 3601–3614.
- [46] ZHU Wen, REN Li, LU Chong, XU Hao, SUN Feng-zhan, MA Zhe-wen, ZOU Jian-xin. Nanoconfined and in situ catalyzed MgH₂ self-assembled on 3D Ti₃C₂ MXene folded nanosheets with enhanced hydrogen sorption performances [J]. ACS Nano, 2021, 15: 18494–18504.
- [47] CUI Jie, LIU Jiang-wen, WANG Hui, OUYANG Liu-zhang, SUN Da-lin, ZHU Min, YAO Zhen-dong. Mg-TM (TM: Ti, Nb, V, Co, Mo or Ni) core-shell like nanostructures: synthesis, hydrogen storage performance and catalytic mechanism [J]. Journal of Materials Chemistry A, 2014, 2: 9645-9655.
- [48] HANG Yi-ke, AN Cui-hua, ZHANG Qiu-yu, ZONG Lei, SHAO Hua-xu, LIU ya-fei, ZHANG Yan, YUAN Huatang, WANG Cai-yun, WANG Yi-jing. Cost-effective mechanochemical synthesis of highly dispersed supported transition metal catalysts for hydrogen storage [J]. Nano Energy, 2021, 80: 105535.

MIL-100(Fe)修饰 TiO2 以高效改善氢化镁的储氢性能

周任1,王李1,钟涛1,李帅1,高东强1,吴富英2,张刘挺1

- 1. 江苏科技大学 能源与动力学院,镇江 212003;
 - 2. 江苏科技大学 分析测试中心,镇江 212003

摘 要: 为了改善氢化镁(MgH2)在固态储氢中热力学稳定、动力学迟缓的问题,采用自组装方法原位合成了 MIL-100(Fe)修饰的 TiO2 纳米片(NS)。制备的 TiO2 NS@MIL-100(Fe)对 MgH2 具有优异的催化效果。MgH2+7%TiO2(质量分数) NS@MIL-100(Fe)复合材料在 200 °C条件下开始释放氢气,与纯 MgH2 相比,初始放氢温度降低 150 °C。此外,改性后的 MgH2在 235 °C下 20 min 内可释放 4%(质量分数)的 H2,脱氢活化能降低到 70.62 kJ/mol。在 100 °C和 3 MPa 条件下,MgH2+7%TiO2 NS@MIL-100(Fe)在 10 min 内吸收 5%(质量分数)的 H2。经过 50 次循环后,复合材料仍能保持 6.62%(质量分数)的可逆容量。TiO2 NS@MIL-100(Fe)中氧空位和多价钛的协同效应是 MgH2 动力学和热力学性能提高的关键因素。

关键词:储氢;氢化镁;氧空位;多价钛;催化机理